Does Molecular Size Matter in Photoinduced Electron Transfer Reactions?

Carlos Serpa and Luis G. Arnaut*

Chemistry Department, University of Coimbra, P-3049 Coimbra Codex, Portugal

Received: April 19, 2000; In Final Form: September 8, 2000

Photoinduced electron transfers (ET) from trimethoxybenzene to excited quinones were studied in polar and apolar solvents by flash photolysis and photoacoustic calorimetry. In apolar solvents, back-ET was also observed. The enthalpy, entropy and volume changes of these ET were measured and compared with those from dimethylaniline to excited pyrene. ET to a triplet quinone in an apolar solvent involves a structural volume increase, indicating the formation of a loose ion pair, whereas ET to the singlet state of pyrene leads to a volume contraction. ET from tetramethylbenzidine to excited C_{60} was also measured in benzonitrile and benzene and the formation of a ground-state complex in benzene was detected. The rates of the photoinduced and back-ET were measured and interpreted with nonadiabatic theories and with the intersecting-state model. It is shown that the size of the reactants has a negligible effect on the kinetics of these reactions and that nonspecific solvent effects are only significant for very exothermic reactions.

1. Introduction

The transfer of an electron between two species, even if it is not accompanied by concomitant bond-breaking−bond-forming processes, is a very important reaction in chemistry and in biology. Outer-sphere electron-transfer reactions (ET) are particularly interesting in photochemistry, because a species becomes a better electron donor or acceptor upon electronic excitation. Photoinduced ET have been extensively studied, both theoretically and experimentally.[1−4] The free energy of a photoinduced ET leading to radical ions in solution is usually estimated using a Born approach and leads to the Weller equation[5]

$$\Delta G_{et} = \left[E_D^{ox} - E_A^{red} + \frac{e^2}{\epsilon}\left(\frac{1}{r_\pm} - \frac{1}{r}\right) - \frac{e^2}{\epsilon' r_\pm}\right]23.06 - E^* \quad (1)$$

where the oxidation potential of the donor (E_D^{ox}) and the reduction potential of the acceptor (E_A^{red}), measured in a polar solvent of dielectric constant ϵ', are expressed in eV and the excited-state energy (E^*) and ΔG_{et} are in kcal/mol; e is the electronic charge ($e^2 = 14.70$ eV Å) and the term containing it takes into account the free energy gained by bringing the two radical ions, of effective radii r_+ and r_- and average radius $r_\pm$, to encounter distance r in the solvent of dielectric constant ϵ. Photoacoustic calorimetry (PAC)[6,7] can be used to measure the heat dissipated in fast photoinduced reactions, because this produces a transient expansion of the medium that is detected as a pressure (or acoustic) wave. However, charge separations may also produce volume changes that are difficult to extract from the actual thermal expansion. Furthermore, eq 1 gives a free energy, whereas photoacoustics measure an enthalpy plus a volume change. Thus, the comparison between eq 1 and photoacoustic measurements may give access to entropy and volume changes. One of the motivations of this work is the use photoacoustics and the electrostatic Gibbs free energy of solvation of an ion (of total charge e) or a point dipole (at the center of a cavity of radius a_0 and whose moment is μ)[8]

$$\Delta G_{el} = -\frac{1}{2}\frac{e^2}{a_0}\frac{\epsilon - 1}{\epsilon} - \frac{\mu^2}{{a_0}^3}\frac{\epsilon - 1}{2\epsilon + 1} \quad (2)$$

to separate enthalpic, volume and entropic contributions to the free energy of a photoinduced ET.

The rates of bimolecular ET increase with the reaction exothermicity until the diffusion-controlled limit is attained at $\Delta G° \approx -10$ kcal/mol. Photoinduced bimolecular ET with $\Delta G°$ -10 kcal/mol usually remain diffusion-controlled in the experimentally accessible range of reaction free-energies, the Rehm−Weller plateau.[9] Depending on the solvent polarity and redox potentials of donor and acceptor, the ions formed following ET may remain associated either as a contact radical-ion pair (CRIP) or as a solvent-separated radical-ion pair (SSRIP). Back-ET occurs in such ion pairs with first-order kinetics. For sufficiently exothermic back-ET, the charge-recombination rates decrease with the exothermicity of the reactions, generating the Marcus inverted region.[10] The reasons sustaining the observation of either the Rehm−Weller plateau or Marcus inverted region have been the subject of a lively debate.[11] The shape(s) of the inverted region(s) has (have) also been controversial. The free-energy dependencies of the rates are not the symmetrical inverted parabola predicted by Marcus. Some authors see them as shallow curves,[12,13] owing to high-frequency quantum modes of intramolecular vibrations, and interpret them using nonadiabatic radiationless transition theories.[14−16] Others distinguish between the dependence described above for SSRIP formed by fluorescence quenching and a linear dependence for CRIP produced by exciting ground-state charge-transfer complexes.[17−19] The latter was related to radiationless transitions in the weak coupling limit.[20,21] The existence of a "double inverted region" was also suggested.[11]

Nonadiabatic radiationless transition theories incorporate the basic features of Marcus theory, namely, the partition of the reaction energy barrier into internal (λ_v) and solvent (λ_s)

* Corresponding author. E-mail: lgarnaut@ci.uc.pt.

10.1021/jp001489l CCC: $19.00
Published on Web 11/08/2000

CHART 1

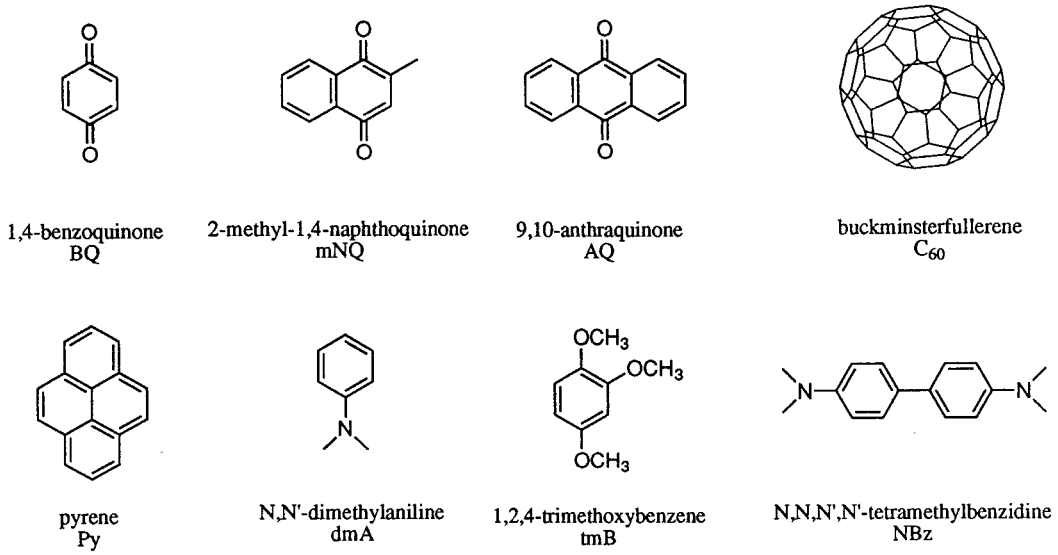

reorganization energies. The latter is given by[22]

$$\lambda_s = e^2\left(\frac{1}{2r_+} + \frac{1}{2r_-} - \frac{1}{r}\right)\left(\frac{1}{n^2} - \frac{1}{\epsilon}\right) \qquad (3)$$

where r is the distance between the centers of the reactants in the activated complex. The solvent reorganization energy should be particularly large for small ions in polar solvents. Additionally, nonadiabatic theories also employ parameters describing low- and high-frequency vibrations, and the electronic coupling between donor and acceptor.

The conventional view that the solvent reorganization energy is the main contribution to energy barrier of ET between organic species in polar solvents was recently challenged and alternative model was proposed.[23] This model, the intersecting-sate model (ISM), was also applied to ET in biological systems.[24−26] Marcus theory and ISM have substantially different predictions concerning the effect of the size of the reactants and polarity of the solvent on ET rates. The second motivation of this work is to test these ET theories using rates measured for reactants with substantially different sizes in solvents with different polarities.

Our PAC measurements resolve sequential heat decays in the nanosecond time scale.[27,28] Levin et al. showed that back-ET in ion pairs originated from the triplet state of quinones are relatively slow.[29−31] Thus, we focus our study on ET to the triplet states of molecules with different sizes from quenchers predicted to give mildly exothermic reactions, Chart 1. We also investigate ET from *N*,*N*-dimethylaniline to pyrene in its singlet state to offer a comparison between singlet and triplet state reactivity using our methodology. Some features of the systems addressed in this study are well established and provide convenient verifications of some of our results. The system ^{3}AQ + tmB was studied in solvents of different polarity,[32,33] $^3C_{60}$ + NBz was studied in polar and nonpolar solvents[34] and ^{1}Py + dmA is one of the most classical of the photoinduced ET systems.[35,36]

2. Experimental Section

2.1. Materials. Spectrograde solvents were used. Benzene was repeatedly washed with sulfuric acid until colorless fractions were separated, then washed with distilled water until neutralization, dried over $CaCl_2$, filtered and distilled over P_2O_5 prior to use. Acetonitrile was first dried over anhydrous KCO_3, refluxed, and then distilled over P_2O_5; the quantity of P_2O_5 was kept below 1% to avoid polymerization of acetonitrile. CCl_4 was first washed with NaOH saturated alcoholic solution, and then with distilled water, dried over $CaCl_2$ and distilled over P_2O_5. Isopropyl ether was first washed with sodium sulfate solution, then with distilled water, dried over $CaCl_2$ and distilled over sodium. Benzonitrile (Aldrich, HPLC grade) was used without further purification. 1,4-Benzoquinone and 2-methyl-1,4-naphthoquinone (Aldrich) were vacuum sublimed. 9,10-Anthraquinone (May & Baker) was recrystallized in toluene. C_{60} (Aldrich, 99%) was used without purification. 1,2,4-Trimethoxybenzene (Aldrich) and *N*,*N*′-dimethylaniline (Merck) were distilled at low pressure, under N_2 atmosphere. *N*,*N*,*N*′,*N*′-tetramethylbenzidine (Aldrich) was recrystallized in a benzene/petroleum ether mixture (7:3). The solutions of C_{60} in benzonitrile were filtered through 0.2 μm pore filters prior to use. The PAC references, 2-hydroxybenzophenone (Aldrich), ferrocene (Merck) and β-carotene (Aldrich), were used without purification.

2.2. Instrumentation and Procedures. All measurements were made at room temperature. The solutions used in fluorescence and lifetime measurements were deaerated by purging with solvent-saturated N_2 for more than 15 min prior to use. The electronic absorption spectra were recorded on a Shimadzu UV-2100 spectrophotometer. Fluorescence and phosphorescence spectra were measured using a Spex Fluorolog 3 with correction for the wavelength dependence of the detection system (RCA C31034 photomultiplier and the 1934D3 module for phosphorimetry).

Our laser flash photolysis (FP) system comprises a Spectra-Physics Quanta-Ray GCR-130 laser, an Applied Photophysics LKS.60 laser flash photolysis spectrometer and a Hewlett-Packard Infinium Oscilloscope (1MS/s). The samples were irradiated either with the second-harmonic (532 nm, 80 mJ, 8 ns fwhm) or with the third-harmonic pulse (355 nm, 50 mJ, 8 ns fwhm) of the Nd:YAG laser. The monitoring white light was produced by a 150 W pulsed Xe lamp. The detection of the transient spectra in the 200−850 nm range was made with Hamamatsu 1P28 and R928 photomultipliers. The lifetime of the pyrene S_1 state was measured with this equipment using its fluorescence mode.

Time-resolved photoacoustic calorimetry (PAC) measurements were performed in a homemade apparatus following the

front-face irradiation design described by Arnaut et al.[6] and reported in detail elsewhere.[27,28] The solutions were pumped through a 0.11 mm thick cell at a 1 mL/min flow with a SSI chromatography pump, and irradiated with an unfocused N_2 laser (1.0 mJ/pulse) working at the frequency of 2 Hz, or with an unfocused PTI dye laser (model PL2300, ca. 0.1 mJ/pulse) pumped by the N_2 laser. Py, mNQ and AQ was irradiated at 337 nm, BQ at 421 nm in CCl_4 and at 337 in benzene, and C_{60} at 500 nm. More than 99% of the light impinging on the front-face dielectric mirror is reflected back in the solution; the rest is transmitted, minimizing the background signal. A small fraction of the laser beam was deflected to a photodiode in order to trigger the digital storage oscilloscope (Tektronix DSA 601, 1 Gs/s, two channels). The acoustic waves generated by nonradiative processes following light absorption in the cell were detected with a 2.25 MHz Panametrics transducer (model A106S), preamplified with a Panametrics ultrasonic preamplifier (model 5676), captured by the transient recorder and transferred to a PC for data analysis. Prior to each PAC experiment, we matched to better than 1% the absorbances of sample and reference at the irradiation wavelength. Measurements at 337 nm used 2-hydroxybenzophenone as photoacoustic reference, whereas at 421 and 500 nm *trans*-β-carotene or ferrocene were used.

One PAC experiment consists of the measuring and averaging of 100 acoustic waves of the sample, reference and pure solvent in the same conditions. Four sets of averaged sample, reference and solvent waves were used for data analysis at a given laser intensity, and four laser intensities were employed in each experiment. These laser intensities were obtained by interposing filters with transmissions in the 27−100% range. The pure solvent signal was scaled by the fraction of light absorbed by the sample in the PAC cell (typically 5%) and subtracted from the sample and reference signals. The deconvolution of background-corrected reference and sample signals gives the fractions of heat deposited and the lifetimes of the corresponding processes. Using the 2.25 MHz transducer, our PAC resolves heat depositions in a time window of a few nanoseconds up to a few microseconds. The shorter heat decays are detected as prompt heat, and are the basis for the choice of calorimetric references: they must deliver all the energy absorbed as prompt heat. Much longer heat depositions do not contribute to the ringing of the transducer. The deconvolutions employed kinetic models consisting of either two or three sequential exponentials and are based on an implementation of the Marquardt algorithm.[37] For each exponential we obtain a lifetime (τ) and a fraction light energy dissipated as heat (ϕ). For example, the heat depositions following the irradiation of quinones in the absence of oxygen and quenchers were deconvoluted using two sequential exponentials, the first one giving the fraction of energy dissipated in the formation of the triplet state (ϕ_1) and the second its decay (ϕ_2). However, ϕ_1 is associated with a lifetime shorter that the time resolution of the experiment and we set its value to $\tau_1 \leq 1$ ns. Thus, we only allow three parameters to vary in the deconvolution. Long-lived triplets do not decay substantially in the time window of the experiment and give meaningless values of ϕ_2 and τ_2. We used three exponentials to deconvolute the heat depositions following the irradiation of a chromophore in the presence of a sufficient quencher to yield quantitative quenching. The first decay gives the formation of the reactive excited state, the second reflects its quenching with the formation of a geminate ion pair, and the third is the recombination of the ion pair. Six parameters are necessary for this deconvolution but we set $\tau_1 = 1$ ns for the reasons discussed above, fix ϕ_1 to the PAC value measured in the absence of quencher, and set τ_2 to the lifetime calculated from the quenching rate measured by FP and the concentration of quencher. Following this procedure, we only allow three parameters to vary in the deconvolution and we can inspect the quality of the deconvolution comparing τ_3 with the ion pair lifetime measured by FP.

3. Theory

3.1. Thermochemistry. Assuming that the ions are incompressible, the electrostatic volume change is the derivative of eq 2 with respect to pressure

$$\Delta V_{es} = \frac{\partial \Delta G_{es}}{\partial p} = -\frac{e^2}{2\epsilon r}\left(\frac{\partial \ln \epsilon}{\partial p}\right)_T \tag{4}$$

Under the same approximation, the electrostatic entropy of solvation is

$$\Delta S_{es} = -\frac{\partial \Delta G_{es}}{\partial T} = \frac{e^2}{2\epsilon r}\left(\frac{\partial \ln \epsilon}{\partial T}\right)_p \tag{5}$$

Incompressible ions have no structural volume changes. We neglect their entropy changes. Thus, the free energy of photoinduced ET leading to free ions can be written

$$\begin{aligned}\Delta G_{et}(\mathrm{FI}) &= -\phi E_{h\nu} + \left(\frac{\rho C_p}{m_w \alpha}\right)\Delta V_{es} - T\Delta S_{es} \\ &= -\phi E_{h\nu} + \frac{e^2}{2\epsilon}\left(\frac{1}{r_+} + \frac{1}{r_-}\right)\left[-\frac{\rho C_p}{m_w \alpha}\left(\frac{\partial \ln \epsilon}{\partial p}\right)_T - T\left(\frac{\partial \ln \epsilon}{\partial T}\right)_p\right]\end{aligned} \tag{6}$$

where $\phi E_{h\nu}$ is the enthalpy + volume change measured by PAC experiments. The factor involving the solvent density (ρ), heat capacity at constant pressure (C_p), molecular weight (m_w) and thermal expansion coefficient (α) is the conversion between molar volumes and energies.[6] Henceforth it will be represented by $K_{VE} = \rho C_p/(m_w \alpha)$.

The pressure and temperature derivatives of incompressible dipoles are, following eq 2,[38]

$$\Delta V_{el} = \frac{\partial \Delta G_{el}}{\partial p} = -\frac{3}{(2\epsilon + 1)^2}\frac{\mu^2}{a_0^3}\left(\frac{\partial \epsilon}{\partial p}\right)_T \tag{7}$$

$$\Delta S_{el} = -\frac{\partial \Delta G_{el}}{\partial T} = \frac{3}{(2\epsilon + 1)^2}\frac{\mu^2}{a_0^3}\left(\frac{\partial \epsilon}{\partial T}\right)_p \tag{8}$$

Furthermore, the structural reaction volume change attending the complexation is

$$\Delta V_{st} = V_{complex} - V_D - V_A \tag{9}$$

The structural entropy change associated with ΔV_{st} can be estimated using one of Maxwell relations, $(\partial S/\partial V)_T = (\partial p/\partial T)_V$,

$$\Delta S_{st} = \frac{\alpha}{\kappa_T}\Delta V_{st} \tag{10}$$

where κ_T is the isothermal compressibility. We can now write

the free energy of a photoinduced ET producing a dipole as

$$\Delta G_{et}(\text{CRIP,ex}) = -\phi E_{h\nu} + \frac{3}{(2\epsilon+1)^2}\frac{\mu^2}{a_0^3}\left[-K_{VE}\left(\frac{\partial\epsilon}{\partial p}\right)_T - T\left(\frac{\partial\epsilon}{\partial T}\right)_p\right] + \left(K_{VE} - T\frac{\alpha}{\kappa_T}\right)\Delta V_{st} \quad (11)$$

This expression is valid for excited-state charge-transfer complexes (exciplexes) and CRIP, given the dipole moment $\mu = e_0 r$, where e_0 is the electronic charge and r is the distance between the two ions.

The free energy of photoinduced ET given by eq 11 can be compared with empirical equations due to Weller and to Gould and Farid. Weller's equation gives the free energy of formation of an exciplex in a solvent of dielectric constant ϵ in terms of their redox potentials in acetonitrile[5]

$$\Delta G_{exc} = \left[E_D^{ox} - E_A^{red} - \frac{\mu^2}{a_0^3}\left(\frac{\epsilon-1}{2\epsilon+1} - 0.19\right) + 0.38\right]23.06 - E^* \quad (12)$$

where we assumed that the destabilization and stabilization energies of typical charge-transfer exciplexes are $U_{stab} \approx U_{dest} \approx 0$.

According to Gould and Farid, the free energy of the photoinduced formation of a CRIP in solution is[39]

$$\Delta G_{CRIP} = \left(E_D^{ox} - E_A^{red} + \frac{0.56}{\epsilon} + 0.003\right)23.06 - E^* \quad (13)$$

which should be compared with eq 12. Identically, for a SSRIP,

$$\Delta G_{SSRIP} = \left(E_D^{ox} - E_A^{red} + \frac{1.52}{\epsilon} - 0.064\right)23.06 - E^* \quad (14)$$

which should be compared with eq 1 when $r \approx 7$ Å.

In this work we compare ΔG_{et}(FI) given by eq 6 with PAC data in polar solvents (acetonitrile and benzonitrile), with the values given by eqs 1 and 14. We also calculate ΔG_{et}(CIP, exc) with eq 11 using our data in less polar solvents (benzene, CCl_4, isopropyl ether) and compare it with the values given by eqs 12 and 13.

3.2. Kinetics. Following the seminal work of Closs and Miller,[40] it became common to interpret inverted-region ET rates using nonadiabatic theories developed in the 1970s. They describe ET rates in terms of the product between an electronic coupling matrix element (V) and a Franck−Condon weighted density of states (FCWD)

$$k_{gr} = \frac{2\pi}{\hbar}V^2\,\text{FCWD} \quad (15)$$

where

$$\text{FCWD} = \sum_{j=0}^{\infty}F_j(4\pi\lambda_s k_B T)^{-1/2}\exp\left[-\frac{(\Delta G_{et} + jh\nu_v + \lambda_s)^2}{4\lambda_s k_B T}\right] \quad (16a)$$

$$F_j = \exp(-S)\frac{S^j}{j!} \qquad S = \frac{\lambda_v}{h\nu_v} \quad (16b)$$

when the vibrations relevant to ET can be represented by one averaged mode, ν_v, resembling carbon skeletal motions of the electron acceptor.[41,42] Early applications of this theory to the free-energy dependence of ET rates between organic molecules involved the fitting of 4 parameters: V, λ_s, λ_v, and ν_v.[29,40,43,44] This number was usually reduced by choosing a value of ν_v in the 1500−2100 cm^{-1} range, compatible with the frequencies of carbon skeletal motions. The coupling matrix element V functions as a scaling factor and its value is determined by the maximum ET rate in a family of reactions, when it is known. The value of λ_s can be calculated by Marcus theory, eq 3, although it is usually fitted to the experimental data, together with λ_v.

More recently, the same authors that established eqs 15−16 as the paradigm to interpret ET rates in the inverted region, have expressed some skepticism concerning their fitting procedures. Closs and Miller concluded that eq 3 is not a reliable guide to the λ_s values needed for eq 16.[45] Gould and Farid observed an increase in reorganization energy with increasing exothermicity.[12,46] Levin realized that eqs 15−16 could not interpret solvent effects on ET rates with constant values of λ_v and ν_v.[31] Vauthey and Jacques showed that a breath of ν_v values from 1200 to 3900 cm^{-1} were necessary to fit the behavior of closely related molecules, such as aromatics and conjugated alkenes, together with λ_v values differing by more than a factor of 2.[47]

Another simple model that has been used to interpret ET rates in a large number of systems in solution[23] and in biological systems[24,25] is the intersecting-state model (ISM). ISM formulates the thermal ET rate in terms of the product between a frequency factor and a nuclear rearrangement term,

$$k_{th} = \upsilon c_0^{1-m}\exp\left(-\frac{\Delta G^{\ddagger}}{RT}\right) \quad (17)$$

where c_0 is the standard concentration ($c_0 = 1$ M) and m the molecularity of the reaction. The nuclear factor is related to the rearrangements of the nuclei from their equilibrium positions in the reactants to their configuration at the transition state. Representing reactants and products by harmonic oscillators of effective force constants f_r and f_p, respectively, the activation free energy for an ET reaction is given by

$$\Delta G^{\ddagger} = \frac{1}{2}f_r d_r^2 \quad (18)$$

where d_r is the bond distortion of the reactant given by the equality presented in Figure 1. The reaction coordinate d is the sum of the bond stretchings (or compressions) of reactants and products from their equilibrium states to their configuration at the transition state, and is given by[48]

$$d = \frac{a'}{2n^{\ddagger}}\ln\left\{\frac{1+\exp(\sqrt{2n^{\ddagger}}\Delta G^0/\Lambda)}{1-[1+\exp(\sqrt{2n^{\ddagger}}\Delta G^0/\Lambda)]^{-1}}\right\}(l_{r,eq} + l_{p,eq}) \quad (19)$$

where a' is a constant ($a' = 0.156$), $n^{\ddagger}$ is the transition state bond order of the reactive bonds, Λ is a parameter that regulates the dissipation of the reaction free energy by the nonreactive modes and $l_{r,eq}$ ($l_{p,eq}$) is the effective equilibrium bond length of the reactants (products). The value of $n^{\ddagger}$ is given by electronic structure of the reactants, because the bond orders are approximately conserved along the reaction coordinate. For example, the carbon skeleton of benzene has 18 bonding electrons distributed by 6 bonds, that is a bond order of 1.5, but its cation lacks one bonding electron so its bond order is 1.42; thus $n^{\ddagger} = 1.46$ for benzene$^{0/+}$. The effective bond lengths, or force constants, of reactants and products in ET reactions

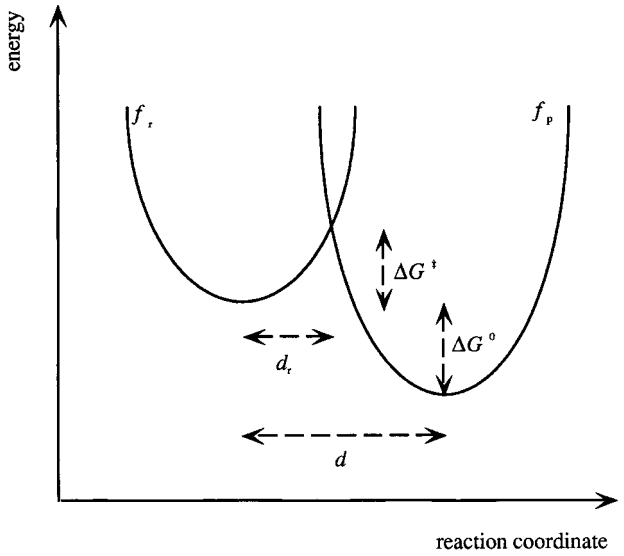

Figure 1. Free-energy profile along the reaction coordinate defined by ISM for an exothermic electron transfer. Reactants and products are represented by harmonic oscillators with force constants f_r and f_p. The parameter d represents the sum of the bond distortions of the bond lengths of the reactants and products from their equilibrium positions to their transition state configuration.

TABLE 1: ISM Reaction Coordinates for the ET of Quinones, Aromatic Amines, and Hydrocarbons[a]

	$f_r = f_p$ (10^3 kcal mol^{-1} Å^{-2})	$l_r + l_p$ (Å)	$n^{\ddagger}$	λ_v (kcal mol^{-1})
$BQ^{0/-}$ *b*	1.05	2.76	1.47	21.6
$tmB^{+/0}$ *c*	0.925	2.79	1.46	19.8
$C_{60}^{0/-}$	0.605[d]	2.87[e]	1.33	16.4
$tmBz^{0/+}$ *f*	0.957	2.80	1.40	22.4
$Py^{0/-}$ *g*	0.901	2.81	1.42	20.6
dmA[h]	0.979	2.79	1.43	21.8

[a] Unless otherwise referenced, the original sources of data can be found in refs 51 and 23. [b] We take this as representative of mNQ and AQ. [c] Taken from benzene. [d] Reference 52. [e] Reference 53. [f] Taken from the relevant bonds of *N,N,N′,N′*-tetramethyl-*p*-phenylenediamine and biphenyl. [g] Taken from anthracene. [h] Taken from the relevant bonds of *N,N,N′,N′*-tetramethyl-*p*-phenylenediamine.

involving organic species are the average of the equilibrium bond lengths, or force constants, of both oxidized and reduced species, $l_{eq} = (l_{red} + l_{ox})/2$ or $f = (f_{ed} + f_{ox})/2$. The effective bond lengths, or force constants, of the oxidized or reduced species are the average of the values of the bonds involved in the reaction coordinate. For aromatic molecules these bonds are those involved in their π-systems. Table 1 presents the data necessary to calculate $\Delta G^{\ddagger}$, except for the parameter Λ. Its value in gas-phase atom-transfer reactions can be estimated from spectroscopic and structural data on the reactants and products,[49] but here we simply use the value previously employed in similar back-ET reactions in CRIP, $\Lambda = 35$ kcal mol^{-1}.[50] The calculation of self-exchange rates does not require Λ, because when $\Delta G^{\circ} = 0$,

$$\Delta G^{\ddagger} = \frac{1}{8} f_r \left[\frac{a' \ln(2)}{n^{\ddagger}} (l_r + l_p)\right]^2 = \frac{\lambda_v}{4} \qquad (20)$$

The vibrational frequency of the reactive bonds in aromatic species ($\nu_n \approx 5 \times 10^{13}$ s^{-1}) is much lower than the electronic frequency ($\nu_{el} \approx 10^{15}$ s^{-1}) and we could expect these reactions to be adiabatic. However, the electron-tunneling probability (χ_{el}) may be much lower than unity and the effective electron frequency may drop below ν_n. We formulate the electron-tunneling probability in terms of the product between a spin and symmetry forbidden factor (χ_0), and a distance-dependent nonadiabatic factor. The electronic nonadiabatic factor is the product between the frequency with which the electron attempts to cross the tunneling barrier and the electron-tunneling probability

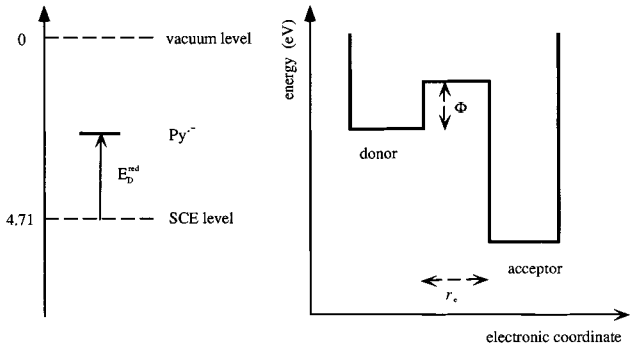

Figure 2. Calculation of the electron tunneling decay coefficient β, for an ET from $Py^{\bullet-}$ to $dmA^{\bullet+}$ as the WKB solution for the probability of tunneling through a square potential energy barrier.

$$\nu = \chi_0 \nu_{el} \exp(-\beta r_e) \qquad (21)$$

where β is the tunneling decay coefficient and r_e is the donor−acceptor separation. A simple but meaningful description of the tunneling barrier separating donor and acceptor is that of a square barrier of width r_e and height Φ, Figure 2.[54] The barrier height Φ is obtained from the energy of the electron in the donor relative to its energy at rest in the vacuum at an infinite separation from the donor, $\Phi_0 = \Phi_{SCE} + E_D^{red}$, where Φ_{SCE} is the absolute potential of SCE ($\Phi_{SCE} = 4.71$ eV),[55] and from the dielectric stabilization of the electron by the medium during the tunneling process, $\Phi = \Phi_0/\epsilon_{op}$.[54] According to the WKB approximation,[56] we have

$$\beta = \frac{4\pi}{h}\sqrt{2m_e\Phi} = \frac{1.025}{n_D}\sqrt{\Phi_0} \qquad (22)$$

where m_e is the electron mass at rest, the optical dielectric constant was equated to the square of the refractive index, $\epsilon_{op} = (n_D)^2$, and the constant is obtained when Φ_0 is expressed in eV and β in Å^{-1}. For example, the energy of the electron in the donor in the $C_{60}/C_{60}^{\bullet-}$ self-exchange is $\Phi_0 = 4.71-0.42$ eV, n_D(benzene) = 1.498 and $\beta = 1.417$ Å^{-1}. With $r_e = 3.5$ Å, we obtain $\nu = 7.0 \times 10^{12}$ s^{-1}, which is appropriate to calculate the spin-allowed ET discussed in this study. Intersystem crossing in aromatic hydrocarbons has a prohibition factor of about 10^6 that distinguishes it from internal conversion.[57,58] This suggests the use of $\chi_0 \leq 10^{-6}$ in spin-forbidden back-ET in quinones and amines.

There are substantial differences between the use of nonadiabatic theories and ISM. The former fits 4 parameters to the energy dependence of ET rates, but it is unlikely that any fitting procedure converges to a unique set of V, λ_s, λ_v, and ν_v. Furthermore, the reorganization energies may not remain constant in the reaction series, because they may increase with the exothermicity. ISM employs only one adjustable parameter (Λ). The value of Λ modulates the increase in reorganization energy with increasing exothermicity, Figure 3. The differences between ISM and Marcus theory are more profound. They assign different roles to the solvent and vibrational modes and adopt different criteria to locate the transition state. A critical assessment of these two theories was recently presented.[23] In

TABLE 2: Properties of the Electron Acceptors Employed in This Study[a]

	solvent	molar volume (Å^3) exp	molar volume (Å^3) calc	E_D^{red} (vs SCE) (V)	E_T (kcal/mol)	Φ_T (PAC)	τ_T (ns) FP	τ_T (ns) PAC
BQ	benzene				52.9		8.7	
	CCl_4	136	102			0.996	1.03×10^3	
	acetonitrile			−0.52[b]		0.983	5.43×10^3	
mNQ	benzene	179	165		58.2	1.03	63	74
	CCl_4						1.61×10^3	
	acetonitrile			−0.77[c]		1.04	0.83×10^3	
AQ	benzene	241	191		63.0	1.06	130	160
	CCl_4						0.78×10^3	
	acetonitrile			−0.95[b]		0.948	1.62×10^3	
C_{60}	benzene	726			36.3[d]	0.933	2×10^4	
	benzonitrile			−0.42[e]		≈1[f]	1×10^4	
Py	isopropyl ether	264	194		77.0[g]		402	200−300
	acetonitrile			−2.10[h]	76.7[g]		315	200−250

[a] The experimental and calculated molar volumes of tmB are 247 and 169 Å^3 (175 Å^3 with a 2.8 Å radius probe) respectively, and of dmA are 211 and 137 Å^3. [b] Reference 60. [c] Reference 61. [d] Reference 62. [e] Reference 63. [f] From the singlet oxygen quantum yield in aerated solutions. [g] S_1 state energy measured by PAC. [h] Reference 64.

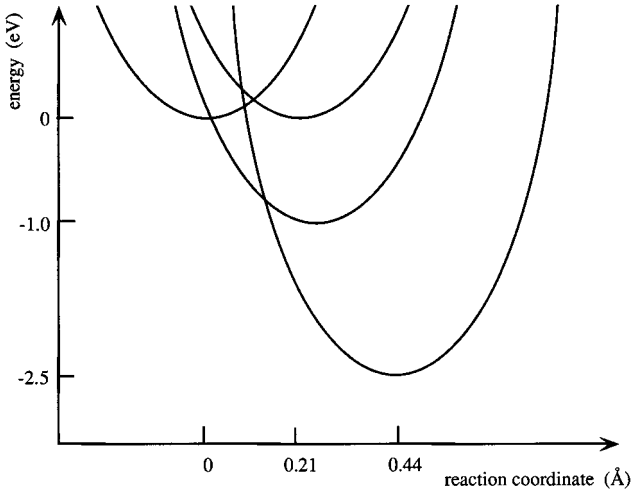

Figure 3. Effect of the reaction free energy on the reaction coordinate of ISM. ISM implicitly accounts for the increase in λ with $\Delta G°$ because the horizontal displacement of the reactant and product curves increases with $\Delta G°$. The location of the maximum depends on the parameters of the reaction coordinate and of Λ ($\Lambda = 35$ kcal mol^{-1} for these ET).

this work we employ two strategies to reduce the number of adjustable parameters of the nonadiabatic theories. We always make $\nu_v = 1600$ cm^{-1} and fit V to the maximum ET rate, but either we look for guidance in Marcus theory to estimate λ_s (eq 3) or we employ ISM to calculate λ_v (eq 20). We also calculate ET rates directly with ISM.

4. Results

The molar volumes of the electron acceptors presented in Table 2 were obtained from the corresponding densities and molecular weights. We also used Connolly surfaces to calculate the volume excluded to a probe sphere of 1.4 Å radius or, in the case of reactions in CCl_4, of 2.8 Å radius. A Connolly surface is the boundary of the volume from which a probe sphere is excluded if it is not to experience van der Waals overlap with the atoms.[59] The volumes obtained by this method are ca. 25% smaller than the molecular volumes. We made no attempt to improve the calculated values by scaling, for instance, the van der Waals interactions. Such a refinement is superfluous given the dramatic simplification of the structure of our solvent molecules. We used a probe radius of 2.8 Å to study the BQ + tmB system in CCl_4 because this is the size of a CCl_4 molecule seen by other CCl_4 molecules using Connolly surfaces. The structures of the (neutral) species were optimized by molecular mechanics prior to the calculation of their volumes.

The triplet energies (E_T) presented in Table 2 were taken from the origin of the quinones phosphorescence at 77 K in toluene. They are in good agreement with literature values.[65] We were unable to detect phosphorescence from the triplet state of C_{60}. Using the external heavy atom effect, Linschitz and co-workers obtained $E_T = 36.3 \pm 0.1$ kcal/mol from the phosphorescence emission threshold at 788 nm.[62] When the relaxation energy of the ground-state species formed by fluorescence is negligible, as is the case for these molecules, we can calculate triplet state quantum yields from[27]

$$\phi_1 = 1 - \frac{E_T}{E_{h\nu}}\Phi_T \tag{23}$$

where ϕ_1 is the fraction of heat deposited in less than 1 ns in our PAC experiments. In all our experiments, we extrapolate ϕ_1 to zero laser intensity from the values measured at four different laser intensities. The triplet quantum yields obtained with this procedure are shown in Table 2. We remark, in particular, the agreement between the value we measured for C_{60} in benzene and the value reported by Linschitz and co-workers, $\Phi_T = 0.93 \pm 0.07$.[66] The fraction of laser energy dissipated as heat by C_{60} in benzonitrile in less than 10 ns was $\phi_1 = 0.55 \pm 0.05$. This apparently indicates a low Φ_T but the average of 16 measurements in air-saturated benzonitrile solutions gave $\phi_2 = 0.23 \pm 0.01$. This can be used in[27]

$$\phi_2 E_{h\nu} = E_T - E_\Delta \Phi_\Delta \tag{24}$$

where E_Δ is the singlet oxygen energy ($E_\Delta = 22.5$ kcal/mol), to calculate a singlet oxygen quantum yield $\Phi_\Delta = 1.00 \pm 0.04$. We interpret the excess of heat measured in the fast decay as a consequence of the turbidity of our solutions in benzonitrile ever after filtration. Light absorption by small particles may lead to fast energy degradation and contribute to ϕ_1.

4.1. Polar Solvents. Table 3 presents the lifetimes of the triplet states measured by flash photolysis in deaerated acetonitrile and benzonitrile solutions. Following the influential work of Kemp and Porter on BQ in water,[67] it has been wrongly assumed that ^{3}BQ has an intrinsically short lifetime.[68] A reinvestigation of this system by Bensasson and co-workers revealed that actual lifetime of ^{3}BQ in water is 530 ns.[69] We measured a short lifetime in benzene, but in CCl_4 and in acetonitrile its lifetime is similar to those of the other quinones,

TABLE 3: Electron Transfer in Acetonitrile ($\epsilon = 35.94$), Except for C_{60} Which Is in Benzonitrile ($\epsilon = 25.2$)[a]

	k_q (M^{-1} s^{-1}) FP	$-\phi_2 E_{h\nu}$ PAC	$K_{VE}\Delta V_{es}$ eq 4	$-T\Delta S_{es}$ eq 5	ΔG°_{et} eq 6	ΔG°_{FI} eq 1, $r = \infty$	ΔG°_{SSRIP} eq 14
^{3}BQ + tmB		−17.9	−3.5	3.3	−18.1	−15.1	−15.6
^{3}mNQ + tmB	1.2×10^{10}	−17.2	−3.4	3.1	−17.5	−14.6	−15.1
^{3}AQ + tmB	1.1×10^{10}	−17.8	−3.2	3.0	−18.0	−15.3	−15.8
$^3C_{60}$ + NTMB	6.7×10^9	−18.7	−4.0	3.0	−19.7	−16.9	−17.0
^{1}Py + dmA	9.8×10^9	−7.8	−3.2[b]	3.0[b]	−8.0	−10.3	−10.8

[a] Energies in kcal mol^{-1}, using K_{VE}(acetonitrile) = 0.30 kcal cm^{-3}, K_{VE}(benzonitrile) = 0.53 kcal cm^{-3}, E_A^{ox}(tmB) = 1.12 V,[70] E_A^{ox}(NBz) = 0.42 V,[65] and E_A^{ox}(dmA) = 0.78 V[64] measured in acetonitrile vs SCE. [b] See text.

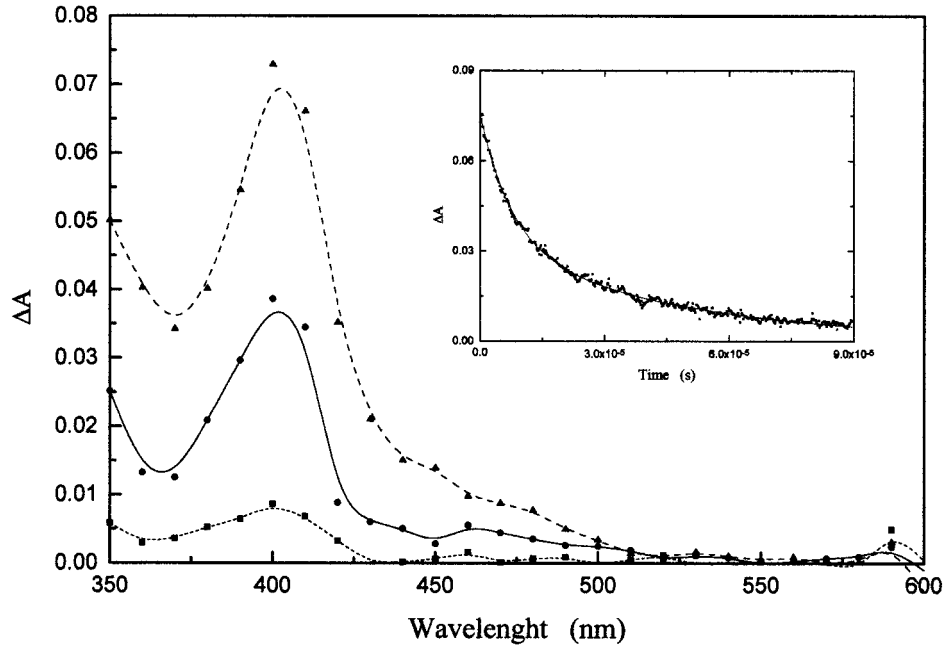

Figure 4. Transient absorption spectrum of BQ in acetonitrile, taken 200 ns (triangles), 10 μs (circles) and 70 μs (squares) after the flash. The inset shows the decay at 400 nm, fitted with $\tau_1 = 7.6$ μs ($A_1 = 0.042$) and $\tau_2 = 47$ μs ($A_2 = 0.033$).

TABLE 4: Electron Transfer in Benzene ($\epsilon = 2.27$), CCl_4 ($\epsilon = 2.24$), and Isopropyl Ether ($\epsilon = 3.88$)

		k_q(M^{-1} s^{-1}) FP	$\phi_2 E_{h\nu}$[a] PAC	$\phi_1 + \phi_2 + \phi_3$ PAC	ΔV_{st}[b] (Å^3)	$\Delta S_{el} + \Delta S_{st}$[c] (cal mol^{-1} K^{-1})	ΔG°_{exc}[a] eq 12	ΔG°_{CRIP}[a] eq 13	τ_{CRIP} (ns) FP	τ_{CRIP} (ns) PAC
^{3}BQ + tmB	benzene						−6.8	−9.3	48.4	
	CCl_4		−23.0	1.11	130	11	−6.8	−9.2	101	74
^{3}mNQ + tmB	benzene	6×10^9	−22.2	1.02	110	10	−6.3	−8.9	268	178
	CCl_4								348	
^{3}AQ + tmB	benzene	9×10^9	−19.9	1.01	85	5	−7.0	−9.5	507	363
	CCl_4								527	
$^3C_{60}$ + NBz	benzene	1.2×10^{10}					−8.6	−11.2		
^{1}Py + dmA	isopropyl ether	5.0×10^9	−3.2 ± 0.4	0.39	−24	−16	−4.2	−7.2	125[d]	122

[a] In kcal mol^{-1}, using the values of E_A^{ox} presented in Table 2. [b] ±10 Å^3. [c] ±5 cal mol^{-1} K^{-1}.

Figure 4. The lifetimes measured by flash photolysis and PAC are in good agreement (Table 2), but, for the reasons discussed above, PAC experiments with the 2.25 MHz transducer do not resolve $\tau_T > 1$ μs. The measured τ_T of C_{60} is certainly limited by insufficient de-oxygenation, but this has no influence in our studies.

The quenching rate constants reported in Tables 3, and also those of Table 4 to be discussed below, were obtained from concentration dependent studies illustrated in Figure 5. They are very close to the diffusion rate constants, as expected from the Rehm−Weller behavior at the corresponding reaction free energies. The ΔG_{et} values obtained by PAC in acetonitrile and in benzonitrile are, after including volume and entropy corrections, ca. 2.5 kcal/mol lower than the values calculated by eq 14 and by eq 1 in the limit of free ions ($r = \infty$). This difference is probably within the combined uncertainties of PAC and electrochemical determinations. Electrostriction entropy and volume changes nearly cancel at room temperature, and the spherical shape implicitly assumed in ΔV_{es} and ΔS_{es} corrections has little impact in our results. We did not recover all the laser energy back into heat ($\phi_1 + \phi_2 < 1$), because long-lived free ions are formed. This is expected in view of the very fast separation rates of geminate ion pairs in acetonitrile, $k_{sep} = 8 \times 10^8$ s^{-1},[71] and of the time window of our PAC experiments. The free energy of the $C_{60}^{\bullet-}$ and $NBz^{\bullet+}$ free ions in benzonitrile should be calculated with their oxidation and reduction potentials in this solvent. However, we have to employ E_A^{red}(NBz) = 0.42 V vs SCE determined in acetonitrile[65] in the absence of data in benzonitrile. This may introduce an appreciable error in the calculation.[72]

The free energy of the $Py^{\bullet-}$/$dmA^{\bullet+}$ ion-pair measured by PAC is 2.5 kcal/mol *higher* than the calculated one. The transient-transient absorption band observed at 490 nm and assigned to

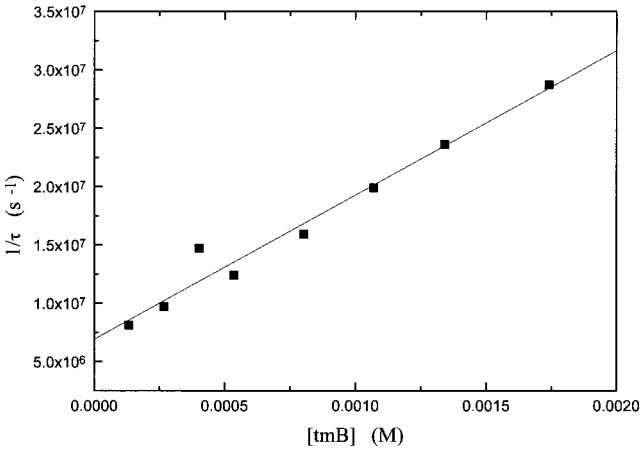

Figure 5. Determination of k_q from the dependence of triplet lifetime on quencher concentrations, illustrated for ^{3}mNQ + tmB in acetonitrile.

$Py^{\bullet-}$ [73] has the same decay time in aerated acetonitrile as the 460 nm band assigned to $dmA^{\bullet+}$ (Figure 6).[74] This is evidence that at least some ions remain associated during our measurements,[75] and their volume and entropy corrections cannot be made as if we were in the presence of free ions.

The distinction between associated and free ions based on their decay times in the presence of oxygen is illustrated in Figure 7. The transient absorption spectrum of AQ in the presence of tmB shows clearly separated peaks corresponding to ^{3}AQ (370 nm), $tmB^{\bullet+}$ (450 nm) and $AQ^{\bullet-}$ (540 nm). The decay lifetime of the former is similar to the growth of the latter. Figure 6 also shows the decays of the radical ions measured in air-saturated acetonitrile or benzene solutions. In benzene the cation and the anion have indistinguishable lifetimes, whereas in acetonitrile the lifetime of $tmB^{\bullet+}$ is much longer. The similar lifetimes of $tmB^{\bullet+}$ and $AQ^{\bullet-}$ in benzene strongly indicate that they remain associated in this solvent, whereas in acetonitrile the cation and the anion have independent behaviors.

4.2. ^{1}Py + dmA in Isopropyl Ether. We observe exciplex luminescence and measure short geminate ion-pair lifetimes in isopropyl ether. This suggests that the geminate ions remain in close proximity and that back-ET limits their lifetimes. This is also expected from thermodynamic considerations and follows from other studies with relate systems.

We interpret our PAC data using three exponentials: the first one accounts for the formation of the singlet state of pyrene, the second one is associated with the quenching step and the last one to back-ET in the exciplex. This kinetic scheme requires the use of 6 parameters in the deconvolution. We reduce the number of parameters to be fitted to the data by imposing some constrains. Using similar Py concentrations and laser intensities in the absence and presence of quenchers, we can set τ_1 and ϕ_1 to the values measured in the absence of quencher. We use the concentration of quencher and k_q to calculate τ_2 and keep it constant in the deconvolution. We are left with three variables (τ_3, ϕ_2 and ϕ_3) that are adjusted in the deconvolution, and an independent verification of our deconvolutions: we must obtain $\tau_3(\mathrm{PAC}) \approx \tau_3(\mathrm{FP})$. Table 4 shows that there is a reasonable agreement between PAC and FP measurements. Figure 8 illustrates the experimental and calculated acoustic waves of this system. We also tested deconvolutions with 2 or 4 variable parameters and obtained essentially the same results.

The volume and entropy corrections associated with exciplex formation in isopropyl ether can be evaluated with eq 11 using $\mu^2/a_0^3 = 0.75$ eV[76] and $K_{VE} = 0.245$ kcal cm^{-3}.[77] This gives $K_{VE}\Delta V_{es} = -5.11$ kcal mol^{-1} and $-T\Delta S_{es} = 3.68$ kcal mol^{-1} at 298 K. Using the difference between these values to correct $\phi_2 E_{h\nu}$ and assuming that the difference between our corrected values and ΔG_{CRIP} is only due to the structural volume change, we obtain $\Delta V_{st} = -24$ Å^3. Furthermore, with this value and eq 10 we obtain, after adding ΔS_{es}, $\Delta S = -16$ cal mol^{-1} K^{-1}. Weller and co-workers obtained $\Delta V_{st} = -26$ Å^3 from pressure dependence of the exciplex fluorescence[38] and $\Delta S_{st} = -18 \pm 1$ cal mol^{-1} K^{-1} from its temperature dependence, in hexane.[5]

Flash photolysis of Py + dmA reveals a band at 419 nm, due to the pyrene triplet state,[78] even when the concentration of dmA reaches 3.3×10^{-2} mol dm^{-3}. At such a high quencher concentration, intersystems crossing from the singlet cannot compete with exciplex formation and the triplet must be generated from the exciplex. Thus, three mechanisms contribute to the decay of the exciplex: intersystem crossing to ^{3}Py, fluorescence emission and back-ET. Energy conservation requires

$$E_{h\nu}\phi_3 = (1 - \Phi_F)(E_{ex} - E_T) + E_T\Phi_{-et} \qquad (25)$$

Using $E_{h\nu} = 84.9$ kcal mol^{-1} from the 337 nm N_2 laser line, $\Phi_F = 0.37 \pm 0.02$ in diethyl ether[79] and $E_T = 48.5$ kcal mol^{-1},[65] we obtain $\Phi_{-et} = 0.13$. This is not strictly true since ϕ_3 includes volume and entropy changes, but the small difference between

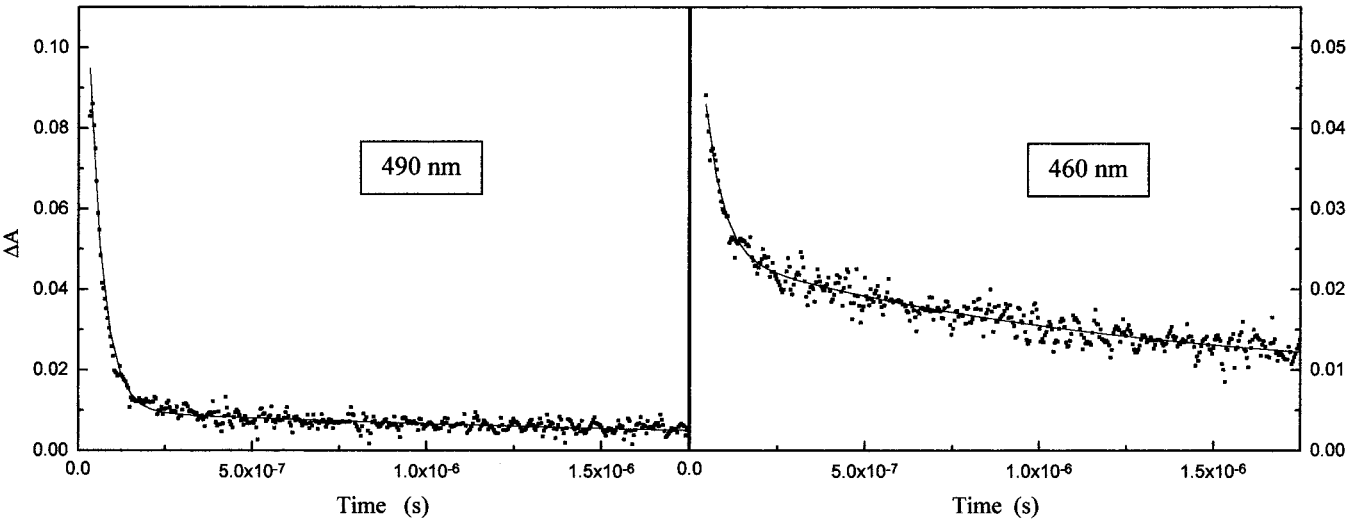

Figure 6. Two-exponential fit of the $Py^{\bullet-}$ (490 nm) and $dmA^{\bullet+}$ (460 nm) decays in aerated acetonitrile. The short-lived decay times are 41 and 49 ns, respectively.

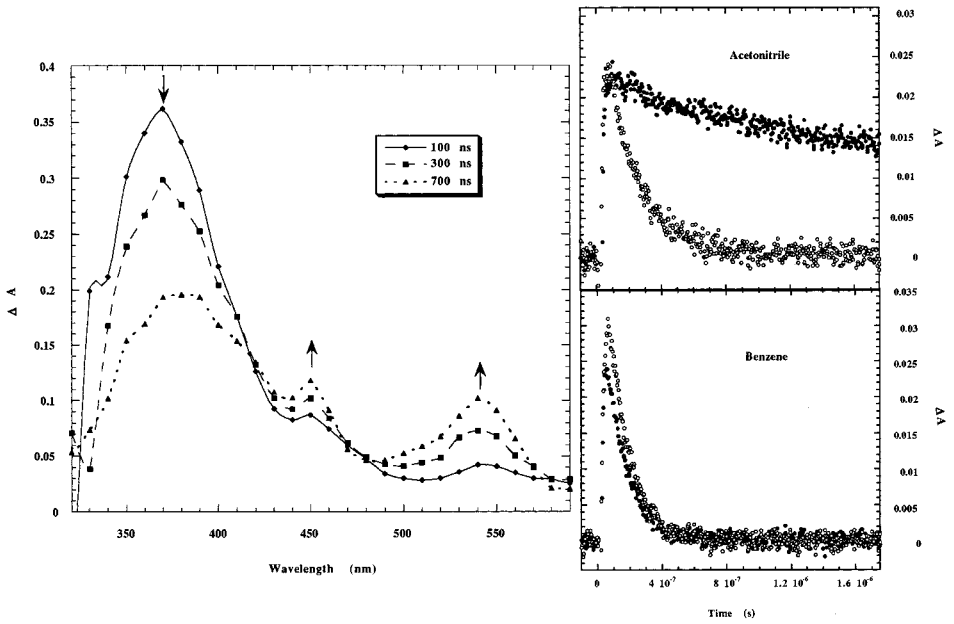

Figure 7. Left panel: transient absorption spectrum of AQ in N_2-saturated acetonitrile in the presence of tmB 1.34×10^{-4} M. Right panels: decays measured at 450 nm ($tmb^{\bullet+}$, closed circles) or 540 nm ($AQ^{\bullet+}$, open circles) in aerated acetonitrile, and at 450 nm ($tmB^{\bullet+}$, closed circles) or 530 nm ($AQ^{\bullet+}$, open circles) in aerated benzene.

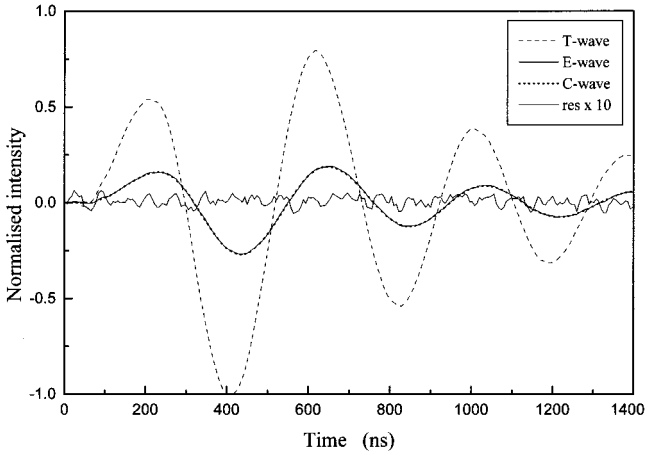

Figure 8. Photoacoustic waves for the system Py + dmA in isopropyl ether. Normalized reference (T-wave) and observed Py + dmA (E-wave) waves, after correction for the background signal (pure isopropyl ether). The C-wave is the convolution between the T-wave and a three-exponential kinetic model ($\phi_1 = 0.1590$, $\phi_2 = 0.0454$, $\phi_3 = 0.1972$, $\tau_1 = 1$ ns, $\tau_2 = 12.3$ ns and $\tau_3 = 109$ ns). Res × 10 = (E-wave − C-wave) × 10.

the exciplex energy and its energy as calculated by ϕ_2, ensures us that the error introduced in Φ_{-et} is less than 0.03. With this value we can now calculate $\Phi_T = 0.50$, $k_{-et} = 1.0 \times 10^6$ s^{-1} and $k_{isc} = 4 \times 10^6$ s^{-1}. Weller and co-workers measured $k_{isc} = 9 \times 10^6$ s^{-1} and 7×10^6 s^{-1} for the same system in methanol and ethanol, respectively.[79]

The excellent agreement between the values of ΔV_{st}, ΔS, and k_{isc} deduced from our experiments and the literature values, shows that our methodology is appropriate to determine the enthalpy, entropy and volume changes associated with exciplex formation.

4.3. ^{3}Quinones + tmB in Benzene and CCl_4. We analyze the PAC data for these systems using the methodology described above. The interpretation of the results obtained with triplet quinones is simpler because the triplet CRIP can only decay by back-ET. Under this conditions we expect that $\phi_1 + \phi_2 + \phi_3 = 1$, in addition to $\tau_{CRIP}(PAC) \approx \tau_{CRIP}(FP)$. Table 4 shows that this is verified.

The energies of CRIP formed in less polar solvents were calculated with eq 12 assuming a full charge separation over a 3.5 Å distance and $a_0 = 7$ Å, that is $\mu^2/a_0^3 = 0.51$ eV. This gives a correction factor of 0.36 eV for benzene, which should be compared with 0.34−0.36 eV measured by Levin et al.[30] The lower limit is obtained with $\mu^2/a_0^3 = 1.0$ eV, that corresponds to a full charge separation over a 4.9 Å distance assuming the same a_0. The electrostriction volume and entropy corrections for CRIP tend to cancel much in the same way as shown before for free ions. For example, $mNQ^{\bullet-}/tmB^{\bullet+}$ in benzene gives $K_{VE}\Delta V_{es} = -2.2$ kcal mol^{-1} and $-T\Delta S_{es} = 1.6$ kcal mol^{-1} with $\mu^2/a_0^3 = 0.51$ eV. We can neglect these corrections and focus on structural reaction volume changes. In Table 4 we present the values of ΔV_{st} calculated under the assumption that the difference between $\phi_2 E_{h\nu}$ and ΔG°_{CIP} can be exclusively assigned to ΔV_{st}. We observe a volume increase associated with the formation of the CRIP. Connolly surfaces yield large volume expansions (50−60 $Å^3$) when we impose a distance ca. 5 Å between tmB and AQ or mNQ with the aromatic rings in parallel (Figure 9). This is less than the observed values but nonetheless indicative of the formation of a loose ion pair. We showed in Table 2 that Connolly surfaces underestimate molecular volumes. Another reason for the difference between the calculated and experimental values can be assigned to the choice of a 1.4 Å radius probe. The volume increase calculated for BQ + tmB with a 2.8 Å radius probe is 80 $Å^3$ at a 7 Å separation, but with the smaller probe the quinone and tmB separate at 6 Å and the volume change drops to zero. The ΔS of the quinone systems presented in Table 4 were calculated with $\mu^2/a_0^3 = 1.0$ eV.

4.4. $^3C_{60}$ + NBz in Benzene. We observe a band at 475 nm, assigned to $NBz^{\bullet+}$, and a band at 740 nm, attributed to $^3C_{60}$, immediately after the 6 ns laser flash. Similar findings have been reported by Ito and co-workers.[34] The intensity of the 475 nm band increases and that of the 740 nm band decreases as we increase the concentration of NBz, Figure 10. Furthermore, the lifetime of the $^3C_{60}$ band depends of the concentration of NBz. This indicates that both static and dynamic quenching occur. Braun and co-workers reported $K_{eq} = 1.4$ M^{-1} for the

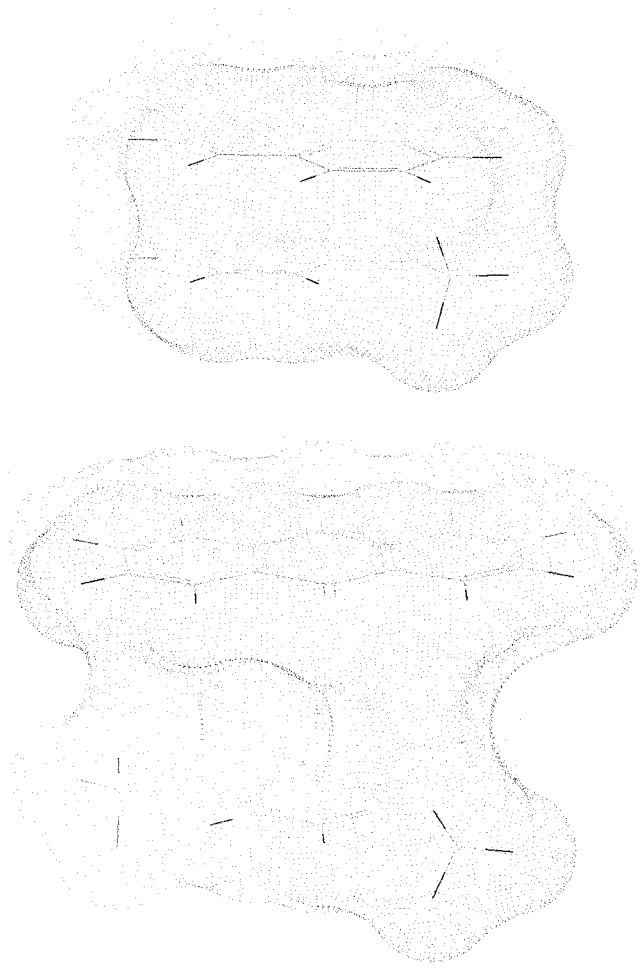

Figure 9. Connolly surfaces for Py + dmA and AQ + tmB.

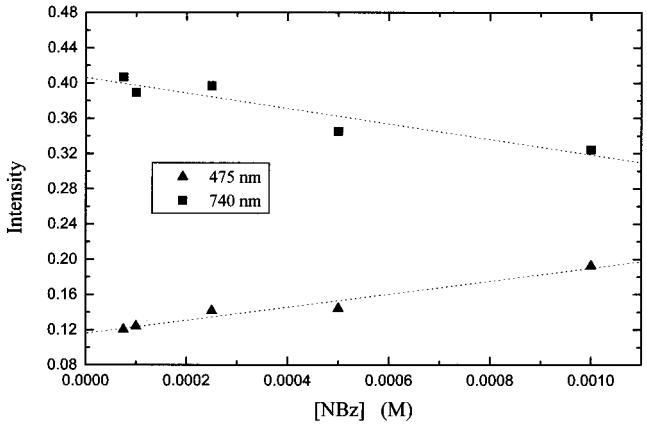

Figure 10. Dependence of the intensity of the 475 and 740 nm bands on the concentration of NBz.

ground-state complex between C_{60} and *N*,*N*,*N*′,*N*′-tetramethyl-1,4-phenylenediamine (TMPD).[80]

Attempts to deconvolute the $^3C_{60}$ + NBz PAC signals in benzene using 3 exponentials showed that either the second or the third exponential was redundant. All the triplet energy of $^3C_{60}$ was lost in the quenching step. This indicates that back-ET is fast relative to triplet quenching. Ito and co-workers reported a back-ET rate constant of 3.3×10^7 s^{-1} in benzene using a NBz concentration of 2.5 mM.[34] We measured the lifetime of the 475 nm band using NBz concentrations in the 0.1−1 mM range; extrapolating the concentration-dependent lifetimes to [NBz] = 2.5 mM, gives the rate reported by Ito et al. The lifetime of $C_{60}^{\bullet-}$/NBz$^{\bullet+}$ depends on the more channels than just back-ET. The recombination rate of the $^3C_{60}^{\bullet-}$ + TMPD$^{\bullet+}$ ion pair in benzene ($\Delta G_{CRIP} = -18.7$ kcal mol^{-1}) is 1.4×10^8 s^{-1} and is not significantly dependent on TMPD concentration.[80]

4.5. ET Kinetics. The measured back-ET rates occur in Marcus inverted region. We can interpret them either using eqs 15−16 of the nonadiabatic theories, or eqs 17−22 of ISM. Levin et al. fitted eqs 15−16 to their data on back-ET in "triplet exciplexes" in benzene using $V = 0.6$ cm^{-1}, $\lambda_s = 0.4$ eV, $\lambda_v = 0.7$ eV and $\nu_v = 1600$ cm^{-1}.[30] These parameters also provide a reasonable fit to the triplet back-ET rates presented in Table 4 and to those reported for $C_{60}^{\bullet-}$/NBz$^{\bullet+}$ and $C_{60}^{\bullet-}$/TMPD$^{\bullet+}$. However, this λ_s is much higher than that given by eq 3, $\lambda_s = 0.01$ eV in benzene,[30] and λ_v is much higher than the value expected from Marcus theory: $\lambda_v = 0.23-0.28$ eV for aromatic hydrocarbons and amines [81,82] and $\lambda_v = 5 \times 10^{-5}$ eV for C_{60}.[83]

Gould et al. fitted eqs 15−16 to back-ET rates in CRIP formed between 1,2,4,5-tetracyanobenzene and alkylbenzenes in chloroform with 660 cm$^{-1} \le V \le 800$ cm^{-1}, 0.7 eV $\le \lambda_s \le$ 0.45 eV, $\lambda_v = 0.31$ eV, and $\nu_v = 1400$ cm^{-1}.[12] The large values of V suggest that an adiabatic approach should be more appropriate, but Gould et al. showed that deep in the inverted region nonadiabatic and adiabatic theories are in quantitative agreement.[84] This value of λ_s is consistent with that expected from eq 3 for the ions under consideration in isopropyl ether and chloroform, $\lambda_s \approx 0.58$ eV. However, back-ET rates in CRIP formed between 2,6,9,10-tetracyanoanthracene and alkylbenzenes in acetonitrile were described by the similar parameters ($V = 1000$ cm^{-1}, $\lambda_s = 0.55$ eV, $\lambda_v = 0.20$ eV and $\nu_v = 1400$ cm^{-1})[84] whereas eq 3 predicts $\lambda_s = 1.11$ eV for acetonitrile. Furthermore, it was recently shown that reorganization energies of $C_{60}^{\bullet-}$ reactions are essentially the same as those of semiquinone radical anions,[83] although from eq 3 one would expect them to be a factor of 4.7 lower.

In summary, Marcus theory does not provide a good guidance to the use nonadiabatic theories because: (i) eq 3 predicts an increase in λ_s from 0.01 to 1.11 eV as we go from benzene to acetonitrile but back-ET in CRIPs have been fitted with a much narrower range of values, (ii) eq 3 predicts an decrease in λ_s with an increase in the size of the ions but C_{60} and quinones have similar λ, and (iii) λ varies with $\Delta G°$.[12,46,85] Thus, we turn to ISM.

Table 1 presented the data required to calculate our ET rates using ISM. With the exception of C_{60}, these data have been extensively employed before.[23,24,51] Aromatic molecules have similar parameters and can be treated as a single family. Here we characterize it by the average data of BQ and tmB data: $f_r \approx f_p = 988$ kcal mol^{-1} Å^{-2}, $l_r + l_p = 2.78$ Å and $n^{\ddagger} = 1.465$. We use $\chi_0 = 1$ for spin-allowed and $\chi_0 = 2 \times 10^{-5}$ spin-forbidden reactions. This prohibition factor is consistent with that estimated by Kasha,[57] considering that our donors and acceptors contain N and O atoms. ISM requires another parameter, Λ, that is constant for a family of reactions. We take its value from earlier studies on back-ET in CRIPs, $\Lambda = 35$ kcal mol^{-1}.[50] The rate constants of bimolecular reactions were corrected for diffusion, $1/k_{obs} = 1/k_{ET} + 1/k_{dif}$, with $k_{dif} = 10^{10}$ M^{-1} s^{-1}. Figure 11 compares the calculated and experimental rates, including the electron exchange between the *tert*-butyl-C_{60} radical adduct (t-Bu$C_{60}^{\bullet}$) and t-BuC_{60}^{-} in benzonitrile/benzene (1:7 v/v), $k_{et} = 1.9 \times 10^8$ M^{-1} s^{-1} at 298 K,[83] and the back-ET rate constants of the $^3C_{60}^{\bullet-}$ + NBz$^{\bullet+}$ and $^3C_{60}^{\bullet-}$ + TMPD$^{\bullet+}$ ion pairs. The quinones and C_{60} belong to the same correlation. Fukuzumi et al. also remarked that the self-exchange

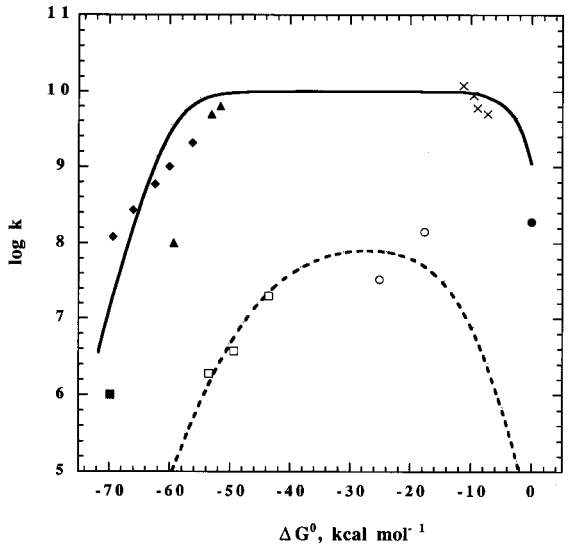

Figure 11. ET rates according to ISM; $f_r \approx f_p = 988$ kcal mol^{-1} Å^{-2}, $l_r + l_p = 2.78$ Å, $n^{\ddagger} = 1.465$, $\Lambda = 35$ kcal/mol and $\chi_0 = 1$ (solid line) or $\chi_0 = 2 \times 10^{-5}$ (dashed line). The calculated rates were corrected for diffusion. The open symbols are back-ET in quinone$^{\bullet-}$ + tmB$^{\bullet+}$ from Table 4 (squares) and $C_{60}^{\bullet-}$ + NBz$^{\bullet+}$ or $C_{60}^{\bullet-}$ + TMPD$^{\bullet+}$ (circles). The solid symbols are ET in Py$^{\bullet-}$/dmA$^{\bullet+}$ (square), tetracyanobenzene$^{\bullet-}$ + alkylbenzenes$^{\bullet+}$ in chloroform (diamonds), tetracyanoanthracene$^{\bullet-}$ + alkylbenzenes$^{\bullet+}$ in acetonitrile (triangles), t-Bu$C_{60}^{\bullet}$ + t-BuC_{60}^{-} self-exchange in benzene/ benzonitrile (circle) and the crosses are k_q from Table 4.

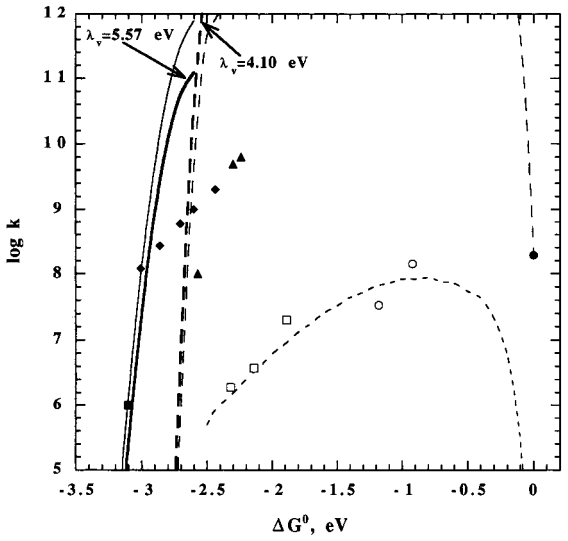

Figure 12. ET rates according to nonadiabatic theories. All the calculations used $\nu_v = 1600$ cm^{-1}. $V = 0.8$ cm^{-1} for spin-forbidden (lower dashed line) and $V = 800$ cm^{-1} for spin-allowed (all other) reactions. The λ_v values of the thick lines are shown in the graph and the thin lines were calculated with $\lambda_v = 0.9$ eV. $\lambda_s = 0.2$ eV for the solid lines and $\lambda_s = 0.05$ eV for the dashed lines. The symbols are described in Figure 10.

rates are essentially the same among C_{60}^{2-}, C_{60}^{-} and the semiquinone radical anions.[83] This is expected from ISM calculations (see Table 1) and verified by the experimental data.

ISM does not separate internal and solvent reorganization energies. It has been argued that nonspecific solvent effects give only a small contribution to the reorganization energy of self-exchanges.[86] The reaction energy of exothermic reactions is dissipated by nonreactive modes, and may amplify the role of the solvent. ISM accounts for this effect in terms of an increase in λ with $\Delta G°$ (Figure 3), that can be estimated from $d(\Delta G°)$. With the reactive bond parameters of our systems and $\Lambda = 35$ kcal mol^{-1}, ISM predicts that λ increases from 0.9 eV for self-exchanges, to $\lambda = 4.15$ eV at $\Delta G° = -2.5$ eV, and $\lambda = 5.77$ eV at $\Delta G° = -3.0$ eV. The fraction of this increase that is associated with the solvent modes can only be estimated using nonadiabatic theories.

We apply eqs 15−16 with $\nu_v = 1600$ cm^{-1}, and $V = 800$ cm^{-1} for spin-allowed or $V = 0.8$ cm^{-1} for spin-forbidden ET in CRIPs. These values are consistent with those of earlier studies and with the prohibition factor estimated by Kasha. We obtain the solvent reorganization energy from the value of λ_s that reproduces the back-ET rate in the ^{1}Py$^{\bullet-}$ + dmA$^{\bullet+}$ ion pair in benzene ($\Delta G_{bET} \approx -3.0$ eV), subject to the restriction $\lambda_s + \lambda_i = 5.77$ eV. As shown in Figure 12, these calculations are not very sensitive to the value of λ_i. Using this method, we obtain $\lambda_s = 0.2$ eV at $\Delta G° \approx -3.0$ eV. At $\Delta G° \approx -2.5$ eV, λ_s drops to 0.05 eV. Lower values of λ_s are expected for less exothermic reactions, but their effect in the calculations becomes negligible. For that reason we employed $\lambda_s = 0.05$ eV and $\lambda_i = 0.9$ eV in the triplet CRIPs calculations. Our separation of solvent and internal reorganization energies also reproduces the self-exchange rate of t-Bu$C_{60}^{\bullet}$ + t-BuC_{60}^{-}. An increase of λ_s by ca. 0.2 eV as the exothermicity increases from 2.5 to 3.0 eV was also proposed by Gould et al.[12]

5. Conclusions

The formation of free ions in acetonitrile involves a volume contraction and a decrease in entropy that, at room temperature, compensate each other in such a way that the enthalpy change measured in PAC is very close to the actual free-energy change, independently of the size of the ions.

ET from tmB to quinones excited to their lowest triplet state in apolar or weakly polar solvents is accompanied by a volume expansion and a small, but positive, entropy of formation. The formation of an exciplex between dmA and Py in weakly polar solvents involves a volume contraction and a decrease in entropy. The ions in the triplet CRIP have distinct transient absorption spectra. We suggest that they are associated in a loose ion-pair with an interplanar separation ca. 2 Å larger than the one of typical exciplexes.

The application of nonadiabatic theories to the rates of back-ET in CRIP using input data from ISM reveals that neither the size of the reactants nor the polarity of the solvent strongly influences the solvent reorganization energy. The solvent reorganization energy of the aromatic molecules studied in this work is less than 5% of the total reorganization energy. Marcus theory overestimates the solvent reorganization energy of these reactions. ISM predicts very similar internal reorganization energies for quinones and C_{60}, and this is experimentally observed. Molecular size plays a minor role in the kinetics of photoinduced ET.

Acknowledgment. We thank Praxis XXI (European Union) for financial support (Project no. Praxis/PCEX/C/QUI/108/96). C.S.S. also acknowledges support from Fundação para A Ciência e A Tecnologia (grant BD/18362/98). We are grateful to Mário T. Rosado (Universidade de Coimbra) for assistance with molecular mechanics calculations.

References and Notes

(1) Chanon, M.; Fox, M. A. *Photoinduced Electron Transfer*; Elsevier: New York, 1988.
(2) Fox, M. A. *Chem. Rev.* **1992**, *92*, 365.
(3) Arnaut, L. G. *J. Photochem. Photobiol. A: Chem.* **1994**, *82*, vii.

(4) Jortner, J.; Bixon, M. *Adv. Chem. Phys.* **1999**, *107*, xv.
(5) Weller, A. *Z. Physik. Chem. N. F.* **1982**, *133*, 93.
(6) Arnaut, L. G.; Caldwell, R. A.; Elbert, J. E.; Melton, L. A. *Rev. Sci. Instrum.* **1992**, *63*, 5381.
(7) Braslavsky, S. E.; Heibel, G. E. *Chem. Rev.* **1992**, *92*, 1381.
(8) Kirkwood, L. G. *J. Chem. Phys.* **1934**, *2*, 351.
(9) Rehm, D.; Weller, A. *Isr. J. Chem.* **1970**, *8*, 259.
(10) Marcus, R. A. *Faraday Discuss. Chem. Soc.* **1960**, *29*, 21.
(11) Arnaut, L. G.; Formosinho, S. J. *J. Mol. Struct. (THEOCHEM)* **1991**, *233*, 209.
(12) Gould, I. R.; Noukakis, D.; Gomez-Jahn, L.; Goodman, J. L.; Farid, S. *J. Am. Chem. Soc.* **1993**, *115*, 4405.
(13) Gould, I. R.; Farid, S. *Acc. Chem. Res.* **1996**, *29*, 522.
(14) Hopfield, J. J. *Proc. Natl. Acad. Sci. U.S.A.* **1974**, *71*, 3640.
(15) Ulstrup, J.; Jortner, J. *J. Chem. Phys.* **1975**, *63*, 4358.
(16) Bixon, M.; Jortner, J. *J. Phys. Chem.* **1991**, *95*, 1941.
(17) Asahi, T.; Mataga, N. *J. Phys. Chem.* **1989**, *93*, 6575.
(18) Miyasaka, H.; Kotani, S.; Itaya, A.; Schweitzer, G.; De Schryver, F. C.; Mataga, N. *J. Phys. Chem. B* **1997**, *101*, 7978.
(19) Mataga, N.; Miyasaka, H. *Adv. Chem. Phys.* **1999**, *107*, 431.
(20) Englman, R.; Jortner, J. *Mol. Phys.* **1970**, *18*, 145.
(21) Freed, K. J.; Jortner, J. *J. Chem. Phys.* **1970**, *52*, 6272.
(22) Marcus, R. A.; Sutin, N. *Biochim. Biophys. Acta* **1985**, *811*, 265.
(23) Formosinho, S. J.; Arnaut, L. G.; Fausto, R. *Prog. Reaction Kinetics* **1998**, *23*, 1.
(24) Arnaut, L. G.; Formosinho, S. J. *J. Photochem. Photobiol. A: Chem.* **1997**, *111*, 111.
(25) Arnaut, L. G.; Formosinho, S. J. *J. Photochem. Photobiol. A: Chem.* **1998**, *118*, 173.
(26) Formosinho, S. J.; Arnaut, L. G. *Res. Chem. Intermed.* **2000**, in press.
(27) Pineiro, M.; Carvalho, A. L.; Pereira, M. M.; Gonsalves, A. M. (d) A. R.; Arnaut, L. G.; Formosinho, S. J. *Chem. Eur. J.* **1998**, *4*, 2299.
(28) Seixas de Melo, S.; Silva, L. M.; Arnaut, L. G.; Becker, R. S. *J. Chem. Phys.* **1999**, *111*, 5427.
(29) Levin, P. P.; Pluzhnikov, P. F.; Kuzmin, V. A. *Chem. Phys. Lett.* **1988**, *147*, 283.
(30) Levin, P. P.; Pluzhnikov, P. F.; Kuzmin, V. A. *Chem. Phys.* **1989**, *137*, 331.
(31) Levin, P. P. *Chem. Phys. Lett.* **1991**, *182*, 663.
(32) Vauthey, E.; Phillips, D.; Parker, A. W. *J. Phys. Chem.* **1992**, *96*, 7356.
(33) Vauthey, E.; Parker, A. W.; Nohova, B.; Phillips, D. *J. Am. Chem. Soc.* **1994**, *116*, 9182.
(34) Ito, O.; Sasaki, Y.; Yoshikawa, Y.; Watanabe, A. *J. Phys. Chem.* **1995**, *99*, 9838.
(35) Taniguchi, Y.; Nishina, Y.; Mataga, N. *Bull. Chem. Soc. Jpn.* **1972**, *45*, 764.
(36) Weller, A.; Staerk, H.; Treichel, R. *Faraday Discuss. Chem. Soc.* **1984**, *78*, 271.
(37) Melton, L. A.; Ni, T.; Lu, Q. *Rev. Sci. Instrum.* **1989**, *60*, 3217.
(38) Pollmann, P.; Rehm, D.; Weller, A. *Ber. Bunseng. Physik. Chem.* **1975**, *79*, 692.
(39) Arnold, B. R.; Farid, S.; Goodman, J. L.; Gould, I. R. *J. Am. Chem. Soc.* **1996**, *118*, 5482.
(40) Closs, G. L.; Calcaterra, L. T.; Green, N. J.; Penfield, K. W.; Miller, J. R. *J. Phys. Chem.* **1986**, *90*, 3673.
(41) Kestner, N. R.; Logan, J.; Jortner, J. *J. Phys. Chem.* **1974**, *78*, 2148.
(42) Fischer, S. F.; Van Duyne, R. P. *Chem. Phys.* **1977**, *26*, 9.
(43) Gould, I. R.; Ege, D.; Mattes, S. L.; Farid, S. *J. Am. Chem. Soc.* **1987**, *109*, 3794.
(44) Vauthey, E.; Suppan, P.; Haselbach, E. *Helv. Chim. Acta* **1988**, *71*, 93.
(45) Johnson, M. D.; Miller, J. R.; Green, N. S.; Closs, G. L. *J. Am. Chem. Soc.* **1989**, *93*, 1173.
(46) Gould, I. R.; Farid, S.; Young, R. H. *J. Photochem. Photobiol. A: Chem.* **1992**, *65*, 133.
(47) Burget, D.; Jacques, P.; Vauthey, E.; Suppan, P.; Haselbach, E. *J. Chem. Soc., Faraday Trans.* **1994**, *90*, 2481.
(48) Varandas, A. J. C.; Formosinho, S. J. *J. Chem. Soc., Faraday Trans. 2* **1986**, *82*, 953.
(49) Pais, A. A. C. C.; Arnaut, L. G.; Formosinho, S. J. *J. Chem. Soc., Perkin Trans. 2* **1998**, 2577.
(50) Formosinho, S. J.; Arnaut, L. G. *J. Photochem. Photobiol. A: Chem.* **1994**, *82*, 11.
(51) Formosinho, S. J.; Arnaut, L. G. *Bull. Chem. Soc. Jpn.* **1997**, *70*, 977.
(52) Inomata, D.; Kutita, N.; Suzuki, S.; Nakao, K. *J. Chem. Phys.* **1995**, *51*, 4533.
(53) Yannoni, C. S.; Bernier, P. P.; Bethune, D. S.; Meijer, G.; Salem, J. R. *J. Am. Chem. Soc.* **1991**, *113*, 3190.
(54) Arnaut, L. G.; Formosinho, L. G. *J. Photochem. Photobiol. A: Chem.* **1996**, *100*, 15.
(55) Heinis, T.; Chowdhury, S.; Scott, S. L.; Kebarle, P. *J. Am. Chem. Soc.* **1988**, *110*, 400.
(56) Bell, R. P. *The Tunnel Effect in Chemistry*; Chapman & Hall: London, 1980.
(57) Kasha, M. *Discuss. Faraday Soc.* **1950**, *9*, 14.
(58) Hunt, G. R.; McCay, E. F.; Ross, I. G. *Aust. J. Chem.* **1962**, *15*, 591.
(59) Connolly, M. L. *Science* **1983**, *221*, 709.
(60) Sasaki, K.; Kashimura, T.; Ohura, M.; Ohsaki, Y.; Ohta, N. *J. Electrochem. Soc.* **1990**, *137*, 2437.
(61) Peover, M. E. *J. Chem. Soc.* **1962**, 4540.
(62) Zeng, Y.; Biczok, L.; Linschitz, H. *J. Phys. Chem.* **1992**, *96*, 5237.
(63) Dubois, D.; Kadish, K. M.; Flanagan, S.; Wilson, L. J. *J. Am. Chem. Soc.* **1991**, *113*, 7773.
(64) Mataga, N.; Asahi, T.; Kanda, Y.; Okada, T.; Kakitani, T. *Chem. Phys.* **1988**, *127*, 249.
(65) Murov, S. L.; Carmichael, I.; Hug, G. L. *Handbook of Photochemistry*; 2nd ed.; Marcel Dekker: New York, 1993.
(66) Biczok, L.; Linschitz, H.; Walter, R. I. *Chem. Phys. Lett.* **1992**, *195*, 339.
(67) Kemp, D. R.; Porter, G. *Proc. R. Soc. London, Ser. A* **1971**, *326*, 117.
(68) Rathore, R.; Hubig, S. M.; Kochi, J. K. *J. Am. Chem. Soc.* **1997**, *119*, 11468.
(69) Ronfard-Haret, J.-C.; Bensasson, R. V.; Amouyal, E. *J. Chem. Soc., Faraday Trans. 1.* **1980**, *76*, 2432.
(70) Zweig, A.; Hodgson, W. G.; Jura, W. H. *J. Am. Chem. Soc.* **1964**, *86*, 4124.
(71) Gould, I. R.; Farid, S. *J. Phys. Chem.* **1992**, *96*, 7635.
(72) Arbogast, J. W.; Foote, C. S.; Kao, M. *J. Am. Chem. Soc.* **1992**, *114*, 2277.
(73) Okada, T.; Karaki, I.; Mataga, N. *J. Am. Chem. Soc.* **1982**, *104*, 7191.
(74) Previtali, C. M. *J. Photochem.* **1985**, *31*, 233.
(75) Orbach, N.; Ottolenghi, M. *Chem. Phys. Lett.* **1975**, *35*, 175.
(76) Beens, H.; Knibbe, H.; Weller, A. *J. Chem. Phys.* **1967**, *47*, 1183.
(77) Marcus, Y. *The Properties of Solvents*; J. Wiley & Sons: Chicester, 1998.
(78) Zanini, G. P.; Montejano, H. A.; Cosa, J. J.; Previtali, C. M. *J. Photochem. Photobiol. A: Chem.* **1997**, *109*, 9.
(79) Werner, H.-J.; Staerk, H.; Weller, A. *J. Chem. Phys.* **1978**, *68*, 2419.
(80) Grzeskowiak, K. N.; Smirnov, S. N.; Braum, C. L. *J. Phys. Chem.* **1994**, *98*, 5661.
(81) Grampp, G.; Jaenicke, W. *Ber. Bunsen-Ges. Phys. Chem.* **1991**, *95*, 904.
(82) Jakobsen, S.; Mikkelsen, K. V.; Pedersen, S. U. *J. Phys. Chem.* **1996**, *100*, 7411.
(83) Fukuzumi, S.; Nakanishi, I.; Suenobu, T.; Kadish, K. M. *J. Am. Chem. Soc.* **1999**, *121*, 3468.
(84) Gould, I. R.; Young, R. H.; Moody, R. E.; Farid, S. *J. Phys. Chem.* **1991**, *95*, 2068.
(85) Gould, I. R.; Noukakis, D.; Gomez-Jahn, L.; Young, R. H.; Goodman, J. L.; Farid, S. *Chem. Phys.* **1993**, *176*, 439.
(86) Formosinho, S. J.; Arnaut, L. G. *J. Mol. Struct. (Theochem.)* **1994**, *130*, 105.